

*Analysis of Hot Spot Asymmetries Using Synthetic X-Ray Images*

**Claire Guo**

Penfield High School

Advisor: Dr. Arijit Bose

Co-advisor: Dr. Reuben Epstein

**Laboratory for Laser Energetics**

University of Rochester

Rochester, NY

January 2018

## **Abstract**

In inertial confinement fusion (ICF) implosions, self-emission x-ray images are used to estimate the hot-spot size and shape. The asymmetry modes of the hot spot can be inferred using these images. Both time-integrated and time-resolved images can be obtained from cryogenic implosion experiments performed on the OMEGA laser. These images are analyzed for the detection of long- and mid-wavelength asymmetries that can be degrading the experiments. This is done by comparison of the experimental images with synthetic images obtained from hydrodynamic simulations. The stagnation phase of implosions is simulated using the 2-D hydrodynamic code *DEC2D*, followed by post-processing using the atomic-physics radiation-transport code *SPECT3D* to produce the synthetic images. From the synthetic images, it is found that the time evolution of the inferred radius and shape of the image differs for implosions with low- and mid-mode asymmetries. This finding can be used to investigate the asymmetry modes degrading the implosion experiments.

## **2. Introduction**

In direct-drive inertial confinement fusion (ICF) [1], multiple high-power laser beams are used to irradiate a deuterium (D) and tritium (T) gas-filled spherical target in order to compress it to high temperatures and pressures. Under these conditions, the fusion of D and T ions is facilitated, leading to energy release. The 60-beam OMEGA laser at the Laboratory for Laser Energetics (LLE), University of Rochester is capable of delivering about 26-30 kJ of energy within a  $\sim 2$  ns pulse duration. This high-power laser is used to routinely perform ICF implosion

experiments. The ultimate goal of ICF research is to produce unlimited clean and safe energy through thermonuclear fusion.

High-intensity laser beams are focused symmetrically on a spherical shell made up of a DT ice layer coated on the inside of a plastic (CH) layer and filled with DT gas. The energy from the laser causes the plastic layer to ablate outward, thereby compressing the DT ice layer and gas fill of the target. This is analogous to rocket propulsion directed spherically inward. The rapid compression of the gas, by a factor of  $\sim 20^3$  in volume within a span of  $\sim 1-2$  ns, heats it up to high temperature. This allows deuterium and tritium nuclei to collide and fuse, each fusion reaction producing an alpha particle, a neutron, and about 17.6 MeV of fusion energy. Initially, the DT shell is accelerated inwards. When the shell nears the origin, it encounters resistance from the hot compressed gas and decelerates.

In a perfect scenario, a spherically symmetric compression of the fuel can lead to significant fusion yields on OMEGA, which have been estimated using simulations. However, nonuniformities arising from several plausible sources can provide initial seeds for the Rayleigh-Taylor instability [2]. During the deceleration phase of an implosion, this instability occurs at the interface of the low-density hot spot (the hot compressed gas) and the high-density shell. The Rayleigh-Taylor instability can introduce growth of compression asymmetries that degrade the fusion yield, relative to the predictions of uniform symmetric calculations. Nonuniformities present on the target are characterized by the mode number  $\ell$ . Targets with two perturbation wavelengths around a great circle will have  $\ell=2$ . Low-mode asymmetries include  $\ell=1-6$  perturbations, mid-mode asymmetries include  $\ell=8-40$  perturbations, and high-mode asymmetries include perturbations with  $\ell>40$ . Different modes can also be combined. For

direct-drive implosions on OMEGA, it is anticipated that the core is degraded by a combination of low and intermediate modes, as shown by Bose *et al.* [3] and Regan *et al.*[4] Although the actual source of the asymmetries is not uniquely identified, low modes can arise from several factors, including long-wavelength DT ice modulations, target positioning, laser beam balance, and laser beam pointing. In addition, the superposition and overlap of all 60 OMEGA laser beams can produce intensity variations that introduce intermediate-mode nonuniformities.

The hot spot produces x-ray emission during the final stages of the compression that can be imaged using x-ray framing cameras. These hot-spot self-emission images can provide information about the symmetry of the hot spot. However, since the hot-spot radius is of the order of  $\sim 20 \mu\text{m}$ , these images are limited by the spatial resolution arising from the imaging optics. In order to better understand these images and identify the specific perturbation modes present in the target during the experiments, the x-ray images are compared with simulated synthetic x-ray images of different modes. The images can be time integrated or time resolved as outlined in Fig. 1.

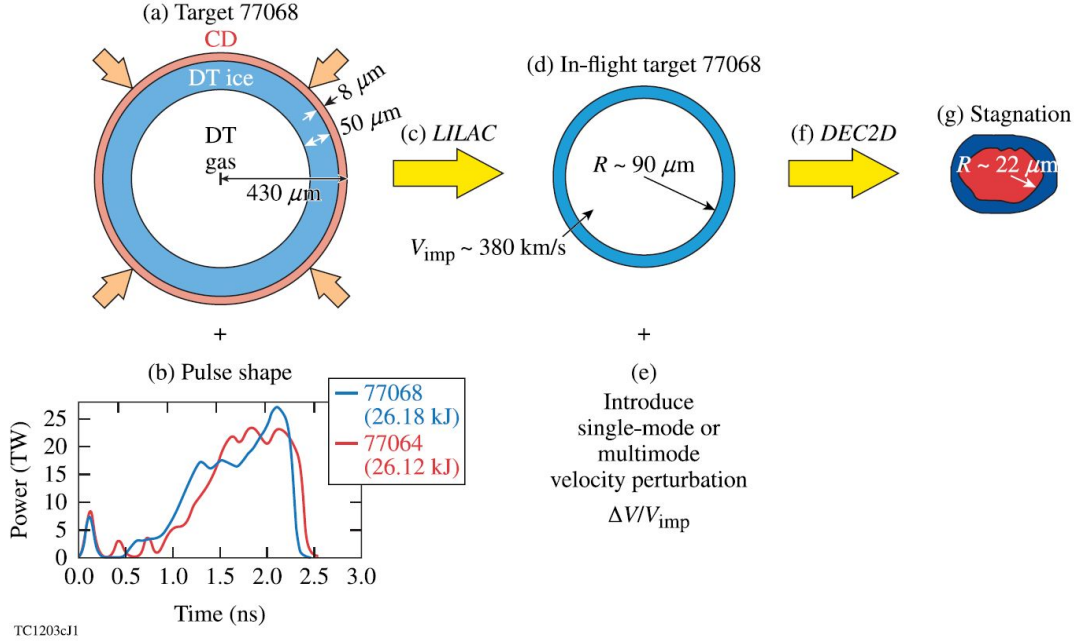


Figure 1: The process of producing synthetic x-ray images for comparison with experiments. The target (a) and pulse shape (b) are used as initial conditions for the 1-D hydrodynamic code LILAC, which is used to (c) simulate the acceleration phase of implosions. The hydrodynamic profiles from the (d) in-flight target simulation are transferred to DEC2D; single- or multimode velocity perturbations are (e) introduced at the inner surface of the shell. (f) The deceleration phase of the implosion is simulated in 2-D. (g) The stagnation parameters are extracted from these simulations.

Synthetic images with different asymmetry modes were processed using DEC2D [5] and SPECT3D [6] calculations. These images were normalized to the maximum intensity for each image and fit with the following function:

$$f(x,y) = e^{-[(x/a)^2 + (y/b)^2]^{\eta/2}}$$

The hot-spot radius  $R_{17}(t)$  is defined by  $R_{17} = \sqrt{a \times b} [-\log(0.17)]^{1/\eta}$ . For a circularly symmetric image,  $R_{17}(t)$  gives the radius where the intensity is 17% of maximum. The index

$\eta(t)$  represents the index of the super-Gaussian fit, with  $\eta = 2$  representing a Gaussian

function. Data such as the time evolution of the hot-spot radius  $R_{17}(t)$  and the super-Gaussian

index  $\eta(t)$  can be used to infer the presence of mid-modes in implosions.

Figure 2 shows an example implosion for which the similarity between the experimental x-ray image and the simulation post-processed image can be seen. Comparison of the experimental images with synthetic images, like in Fig. 2, provides a tool to investigate the asymmetries that are degrading the experiments. The similarities between Images (b) and (c) and both line-outs in Image (d) demonstrate the validity of the synthetic reconstructions.

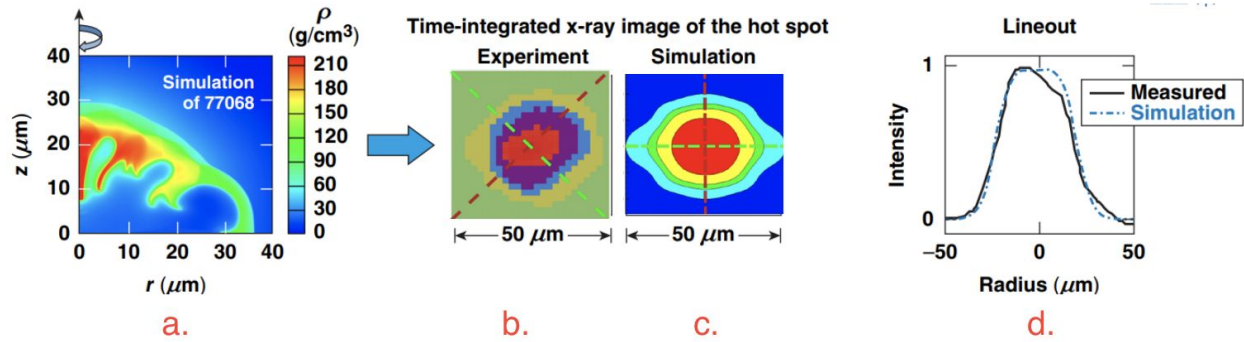


Figure 2: Comparison of synthetic images with the experimental images. Image (a) shows the DEC2D simulation of the shot 77068. Image (b) shows the time-integrated x-ray image from the experiment and image (c) shows the SPECT3D generated synthetic image. Image (d) is a plot of the line-outs taken from the red dashed line of Image (b) and the green dashed line of Image (c).

### 3. Application of the image processing procedure

#### Case 1: Symmetric implosion simulations

Synthetic images for symmetric implosion simulations, i.e. without any seed velocity perturbation, were produced from *DEC2D* and *SPECT3D*. An example is shown in Fig. 3. These images were used to study the relationship between the target density profile and the x-ray emission. Lineouts were taken along the x- and y- axes of the synthetic x-ray image, in order to plot the relationship between normalized intensity and radius and to calculate the super-Gaussian index.

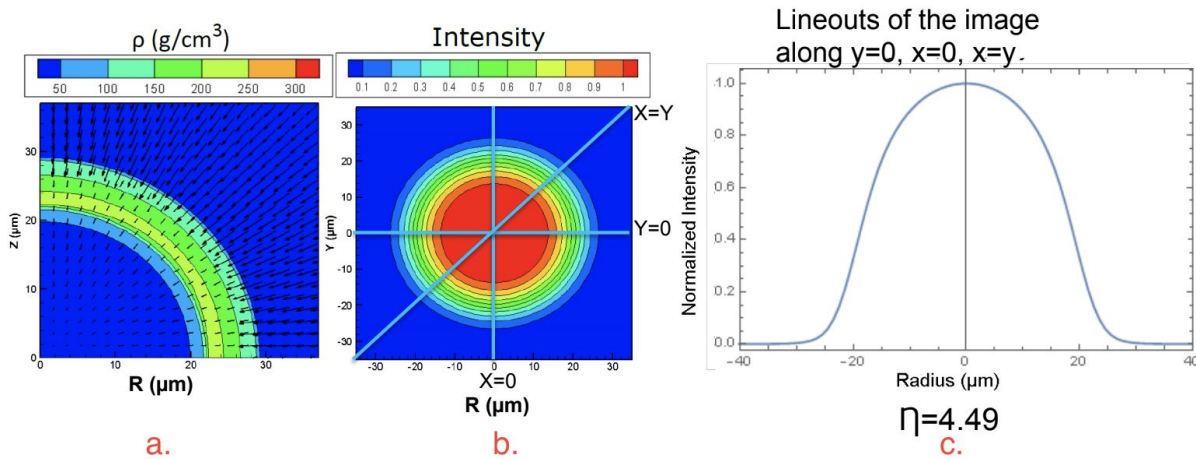


Figure 3: Simulation results for a symmetric implosion (mode 0). (a) is a contour plot of density (g/cm<sup>3</sup>) in the (R,Z) plane, (b) is a time-integrated simulated SPECT3D image, and image (c) is a graph of normalized intensity vs. radius from line-outs taken along y=0, x=0, and x=y from (b). The super-Gaussian index is found to be 4.49. The y-axis of (b) corresponds to the z-axis of symmetry of the simulation (a). Clean SPECT3D images are used to calculate the hot-spot radius and super-Gaussian index.

Image (a) shows that the density profile is symmetric and Image (b) shows that the target is evenly compressed with the maximum intensity of the hot spot being centralized in the middle of the target. The lineouts seen in Fig. 3 (c) are also uniform and identical.

This process of image development was repeated three more times for low, mid, and combination-mode targets. The new images with perturbations were compared to that of the clean simulation of Fig. 3 in order to study the effect of different Rayleigh-Taylor instability modes on an implosion.

#### *Case 2: Simulations with low-mode asymmetry*

Low-mode ( $\ell=2$  asymmetry) was introduced in the DEC2D simulation. The resulting density contour plot is shown in Fig. 4(a). The x-ray image produced using *SPECT3D* is shown in Fig. 4(b). Compared to the images seen in Fig. 3, the images in Fig. 4 are less uniform because of the asymmetry.

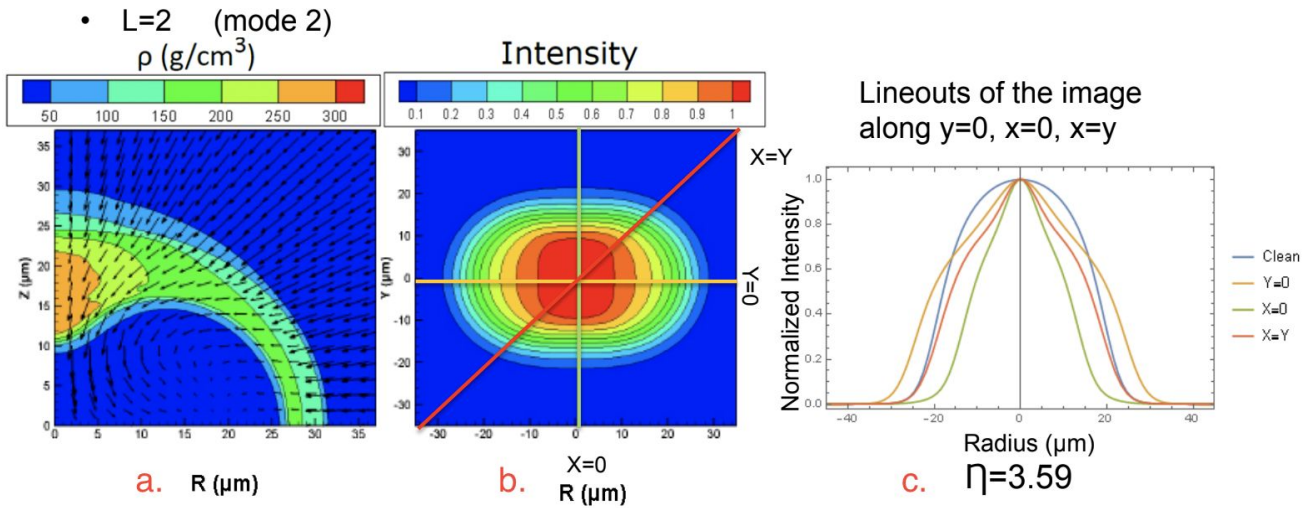


Figure 4: Simulation results for a low-mode (mode 2) implosion. (a) is a contour plot of density ( $\text{g/cm}^3$ ) in the  $(R, Z)$  plane, (b) is a time-integrated simulated SPECT3D image, and image (c) is a graph of normalized intensity vs. radius from line-outs taken along  $y=0$ ,  $x=0$ , and  $x=y$  from (b). The super-Gaussian index is found to be 3.59. The  $y$ -axis of (b) corresponds to the  $z$ -axis of symmetry of the simulation (a). SPECT3D images are used to calculate the hot-spot radius and super-Gaussian index.

Areas of greater density are centralized on the upper and lower areas of the target shell. The resulting intensity contours of Fig. 4(b) are close to elliptical in shape. The lineouts taken in Image (c) are slightly more peaked in the center than that for the clean simulation. This causes the super-Gaussian index to decrease from the 4.49 of Fig.3(c) to 3.59.

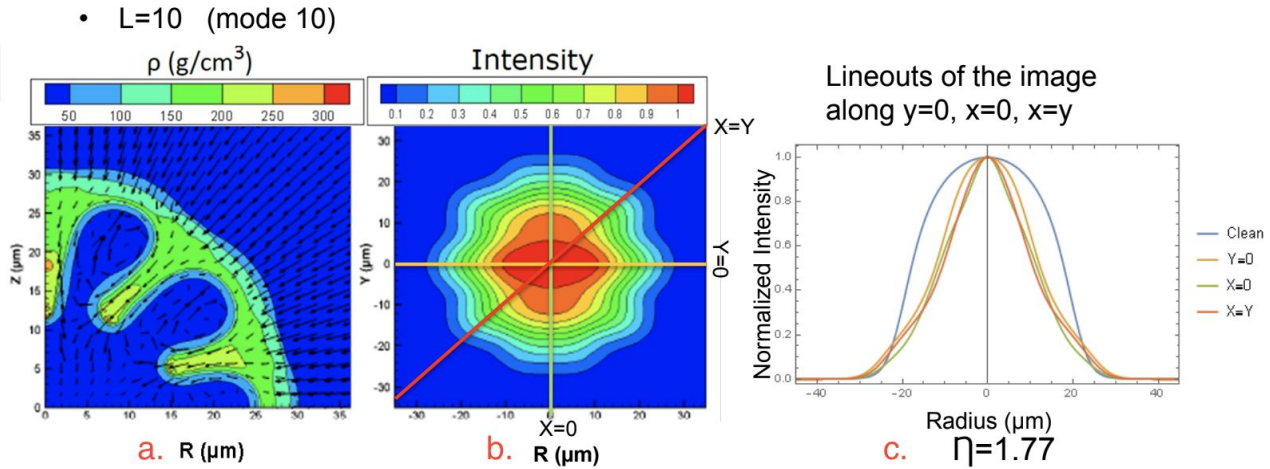


Figure 5: Simulation results for a mid-mode (mode 10) implosion. (a) is a contour plot of density ( $\text{g}/\text{cm}^3$ ) in the  $(R, Z)$  plane, (b) is a time-integrated simulated SPECT3D image, and image (c) is a graph of normalized intensity vs. radius from line-outs taken along  $y=0$ ,  $x=0$ , and  $x=y$  from (b). The super-Gaussian index is found to be 1.77. The  $y$ -axis of (b) corresponds to the  $z$ -axis of symmetry of the simulation (a). SPECT3D images are used to calculate the hot-spot radius and super-Gaussian index.

### Case 3: Simulations with mid-mode asymmetry

A DEC2D simulation with a mid-mode asymmetry ( $\ell=10$ ) was post-processed using SPECT3D. The resulting density contour plot is shown in Fig. 5(a). Compared with that in Fig. 3(a), the density contours show significant structure. Areas of greater density begin traveling into the middle of the target and more density variations occur on the target shell, compared to clean and low-mode simulations. The target has compressed so that there are peaks and troughs on the inner surface instead of it being compressed smoothly into a sphere or an ellipse. The SPECT3D image of Fig. 5(b) mirrors the structure seen in the density contour plot of Fig. 5(a). The lineouts taken in Image (c) are more strongly peaked at the center than the clean and low-mode lineouts. This causes the super-Gaussian index to decrease substantially from the 4.49 of the symmetric case of Fig. 3(c) to 1.77. There is also less variation between the three lineouts.

Case 4: Simulations with combination of low- and mid-mode asymmetry

X-ray images for a simulation with both mode 2 and mode 10 perturbations were processed. These images were used to study how a combination of two modes would affect the properties of the x-ray images.

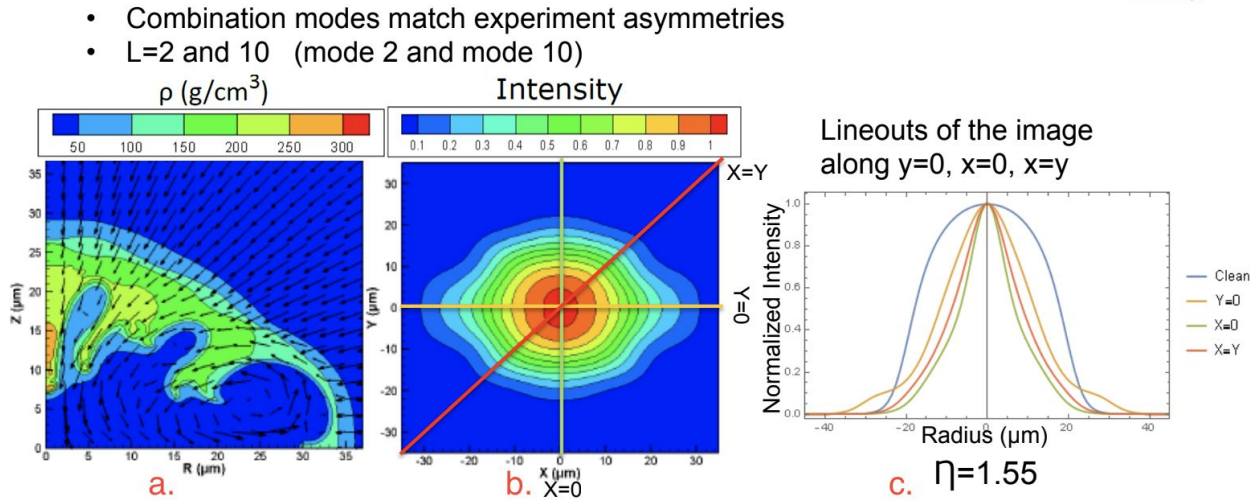


Figure 6: Simulation results for a combination-mode (mode 2 and 10) implosion. (a) is a contour plot of density (g/cm<sup>3</sup>) in the (R,Z) plane, (b) is a time-integrated simulated SPECT3D image, and image (c) is a graph of normalized intensity vs. radius from line-outs taken along  $y=0$ ,  $x=0$ , and  $x=y$  from (b). From (c), the super-Gaussian index is found to be 1.55. The y-axis of (b) corresponds to the z-axis of symmetry of the simulation (a). SPECT3D images are used to calculate the hot-spot radius and super-Gaussian index.

Compared with those in Figs. 3, 4, and 5, the density structures in Fig.6(a) are distributed unevenly around the target. Areas of greater density are located on the upper and lower areas of the target and travel into the middle of the target. The target has compressed so that the target is stretched in the R direction. The intensity image in Fig. 6(b) is similarly stretched. The lineouts taken in Image (c) show a combination of the variability seen in Fig. 4(c) and the narrowing at

the center seen in Fig. 5(c) and are more strongly peaked at the center than the clean, low-mode, and mid-mode lineouts. This causes the super-Gaussian index to decrease further to 1.55.

#### 4. Time evolution history of the hot-spot size

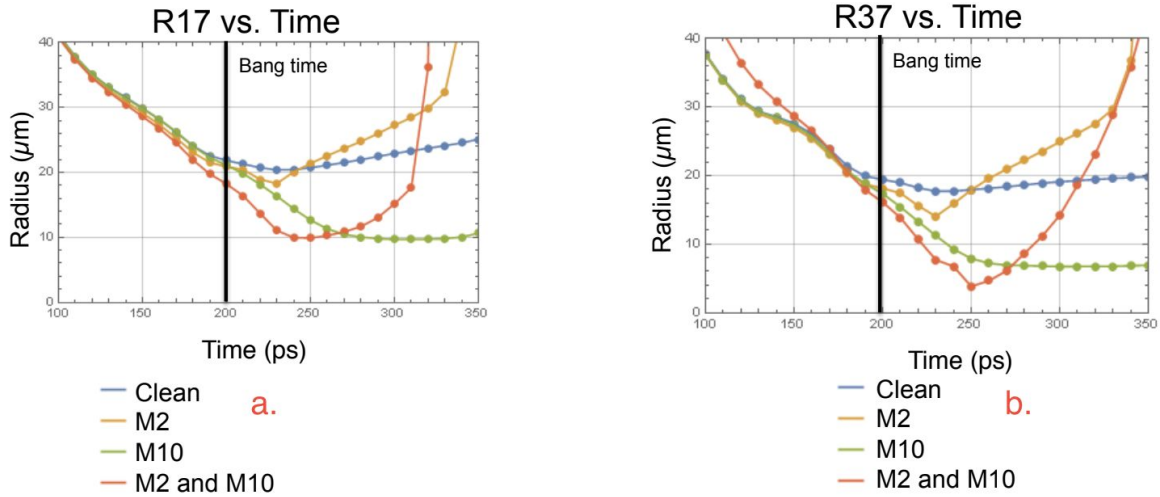


Figure 7: Graphs of (a) radius  $R_{17}$  and (b) radius  $R_{37}$  as functions of time.

The hot-spot radius  $R_{17}$  and the radius  $R_{37} = \sqrt{a \times b} [-\ln(0.37)]^{1/\eta}$  at 37% of maximum intensity are plotted as functions of time in Fig. 7. This figure shows how these radii change over time for different perturbation modes. When compared with data from experimental implosions, the data from these graphs can be used to infer the presence of different perturbation modes.

## 5. Time evolution history of the super-Gaussian index

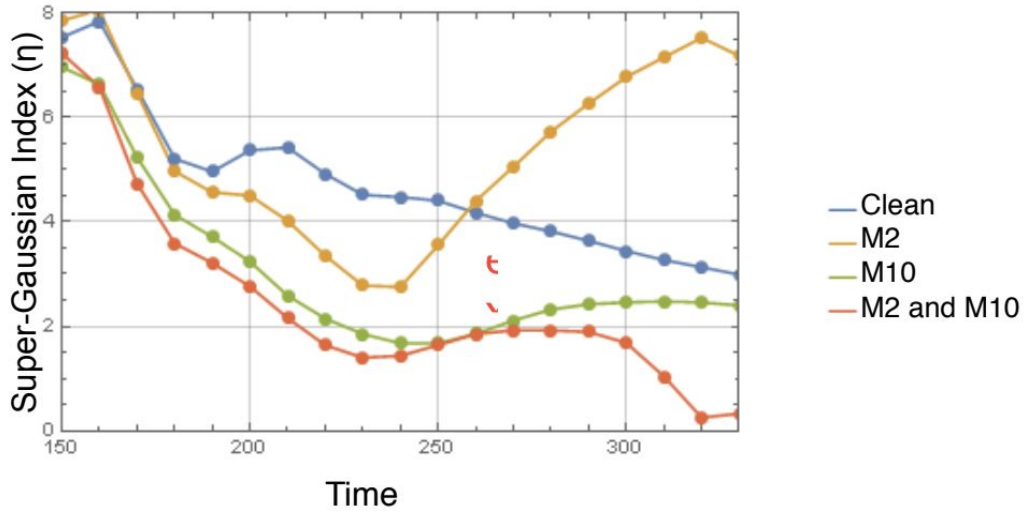


Figure 8: Graph illustrating the relationship between super-Gaussian index ( $\eta$ ) and time (ps)

From the SPECT3D images produced, the super-Gaussian index for the clean, mode 2, mode 10, and combination modes was isolated and plotted in Fig. 8. Fig. 8 shows that the super-Gaussian index decreases at the end of the implosion during laser shots with combination mode perturbations located on the target. These results provide a preliminary indication that the time dependence of the mode-number content and the super-Gaussian index are related. Through comparison with data from experimental implosions, relationships such as this may be used to infer the presence of perturbations of different mode numbers.

## 6. Conclusion

SPECT3D synthetic x-ray images are used to analyze asymmetries of the hot spot. Detection of mid-mode asymmetries in implosions is challenging. However, the synthetic x-ray images produced through this study are effective as a means for understanding the shape of

target profiles with perturbations of different mode numbers over the course of a target implosion. In addition, the time evolution of the hot-spot radius and the super-Gaussian index appear to be related, allowing the presence of mid modes in implosions to be inferred through comparisons with similar data from experimental implosions. These techniques can be implemented to better understand target perturbations, diagnose experimental implosions for potential issues, and analyze target compression over the course of the implosion.

## **7. Acknowledgements**

This project would not have been possible without the help of my advisors, Dr. Arijit Bose and Dr. Reuben Epstein, whose patient support and assistance have guided me along the entire process. I would like to thank Dhruvir Patel, who guided me through producing the synthetic images, and Alison Christopherson who provided the data used to create my images. I would also like to thank Dr. Craxton for providing me with the wonderful opportunity to participate in the LLE high school program and conduct this research project. Finally, I would like to thank the Laboratory for Laser Energetics for this amazing learning experience.

## 8. References

- [1] R.S. Craxton *et al.*, "Direct-Drive Inertial Confinement Fusion: A Review," *Physics of Plasmas* **22**, 110501 (2015).
- [2] D.H. Sharp, "An Overview of Rayleigh-Taylor Instability," *Physica D.* **12**: 3–18 (1948).
- [3] A. Bose *et al.*, "The Physics of Long- and Intermediate-Wavelength Asymmetries of the Hot Spot: Compression Hydrodynamics and Energetics," *Physics of Plasmas* **24**, 102704 (2017)
- [4] S. Regan *et al.*, "Demonstration of Fuel Hot-Spot Pressure in Excess of 50 Gbar for Direct-Drive, Layered Deuterium-Tritium Implosions on OMEGA," *Phys. Rev. Lett.* **117**, 025001 (2016).
- [5] A. Bose *et al.*, "Hydrodynamic Scaling of the Deceleration-phase Rayleigh-Taylor Instability," *Phys. Plasmas* **22**, 072702 (2015)
- [6] J. J. MacFarlane, I. E. Golovkin, P. Wang, P. R. Woodruff, and N. A. Pereyra, "SPECT3D—A Multi-Dimensional Collisional-Radiative Code for Generating Diagnostic Signatures Based on Hydrodynamics and PIC Simulation Output," *High Energy Density Phys.* **3** (1-2), 181-190 (2007).